PHOTONICS Research

Disorder-protected quantum state transmission through helical coupled-resonator waveguides

JungYun Han,[1,2] Andrey A. Sukhorukov,[3] and Daniel Leykam[1,2,*]

[1]Center for Theoretical Physics of Complex Systems, Institute for Basic Science, Daejeon 34126, South Korea
[2]Basic Science Program, University of Science and Technology, Daejeon 34113, South Korea
[3]ARC Centre of Excellence for Transformative Meta-Optical Systems (TMOS), Nonlinear Physics Centre, Research School of Physics, The Australian National University, Canberra, ACT 2601, Australia
*Corresponding author: dleykam@ibs.re.kr

Received 17 June 2020; revised 6 August 2020; accepted 7 August 2020; posted 10 August 2020 (Doc. ID 399919); published 28 September 2020

We predict the preservation of temporal indistinguishability of photons propagating through helical coupled-resonator optical waveguides (H-CROWs). H-CROWs exhibit a pseudospin-momentum locked dispersion, which we show suppresses on-site disorder-induced backscattering and group velocity fluctuations. We simulate numerically the propagation of two-photon wave packets, demonstrating that they exhibit almost perfect Hong–Ou–Mandel dip visibility and then can preserve their quantum coherence even in the presence of moderate disorder, in contrast with regular CROWs, which are highly sensitive to disorder. As indistinguishability is the most fundamental resource of quantum information processing, H-CROWs may find applications for the implementation of robust optical links and delay lines in the emerging quantum photonic communication and computational platforms. © 2020 Chinese Laser Press

https://doi.org/10.1364/PRJ.399919

1. INTRODUCTION

Topological photonics is emerging as a way to create disorder-immune waveguides for light using edge modes of media with nontrivial topological properties [1–3]. Since the first proof-of-concept experiments using gyro-magnetic microwave photonic crystals [4,5], various approaches have emerged to demonstrate topological transport at different length and energy scales [2,3]. Moreover, this field is developing by harmonizing with existing subfields of photonics, i.e., exploring the role of topology in nonlinear optical effects [6], dynamically modulated systems [7], lasers [8–10], and other non-Hermitian systems with structured gain and loss [11].

One promising application of topological photonics is the robust generation and transport of quantum state of light [12–15]. It is a more challenging problem, as the preservation of quantum properties, such as indistinguishability, depends on the phase information, which is often not robust against disorder even for topological edge states [16]. Protecting indistinguishability has turned out to be important, as it provides a desirable resource in quantum technologies to generate entanglement [17]. In optical delay lines, indistinguishability is determined by the degree of temporal overlap, as depicted in Fig. 1. An obstacle to preservation of temporal overlap through standard delay lines is disorder, which can not only induce backscattering and Anderson localization of propagating waves but also destroy information related to the relative phase, which occurs due to the dephasing of the ensemble-averaged state [18,19].

A potential solution is to use the robustness of topological edge states to protect quantum states of light [13,20–23]. For example, photonic quantum spin-Hall phases host bi-directional edge states, which are protected against backscattering by time-reversal and internal (e.g., crystalline) symmetries. Quantum spin-Hall edge states were demonstrated in 2D silicon ring resonator arrays, where the circulation direction within the rings plays the role of spin [24–27]. Other approaches introduce sublattices as a pseudospin degree of freedom emulating real spins [28,29]. The quantum spin-Hall phase supports transport and is robust against certain types of disorder, as backscattering requires a spin flip.

Thus far, topologically protected waveguiding has been largely demonstrated in two or higher dimensional photonic systems, while 1D topologically protected transport has required synthetic dimensions [30] or time modulation such as adiabatic pumping [31]. There is another approach to achieve disorder-resistant waveguiding in 1D without a topological bandgap, based on directly implementing a spin-momentum locked dispersion by breaking time-reversal symmetry, which has been demonstrated using 1D electronic quantum wires [32]. Recently, we proposed a model of a quasi-1D coupled-resonator optical waveguide (CROW) exhibiting a similar helical spin-momentum locked dispersion (H-CROW), by combining circulation direction and sublattice spin-like degrees

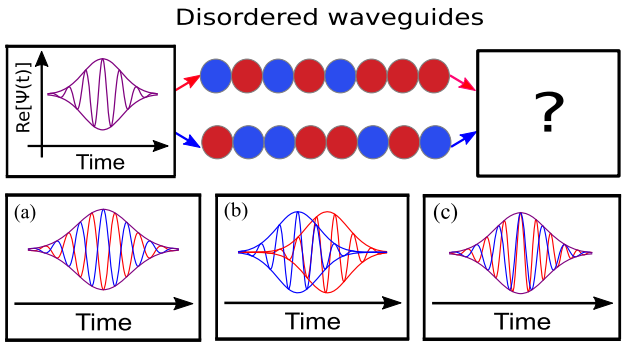

Fig. 1. Temporally indistinguishable photons within the temporal resolution δt propagating through different delay lines can be temporally distinguishable given the delay provided by the ring resonator waveguides is sensitive to disorder, i.e., random red or blue shifts of the individual resonators. Insets below illustrate various possible effects of disorder: (a) phase shift via the difference in phase velocities, (b) difference in arrival times due to variation of the group velocities, and (c) wavepacket distortion due to higher-order dispersion and wavelength-dependent reflection.

of freedom. The former effectively breaks time-reversal symmetry, while the coupling between different sublattices can be tuned to create a sublattice-momentum locked dispersion relation [33]. This results in a suppression of backscattering and enhancement of localization length compared with the regular CROW model as well as preservation of phase information. It is noteworthy, as it provides the way to miniaturize a disorder-resistant waveguide by inducing helical transport.

In this paper, we study the propagation of quantum states of light through H-CROWs and demonstrate that temporal indistinguishability can be robust against moderate disorder, thereby enabling the protection of entangled states. First, in Section 2, we compute the delay time distribution of single-photon states propagating through disordered H-CROWs and find that, for a given disorder strength, H-CROWs yield a narrower distribution of delays compared with regular CROWs. Thus, the temporal overlap of photons travelling along different paths can be preserved. In Section 3, we compute coincidence probability as a witness of indistinguishability and show the Hong–Ou–Mandel (HOM) dip [34]. We then study in Section 4 the propagation of a path-entangled photonic state (N00N state) and show that H-CROWs protect their entanglement. We quantify their purity, associated with an inverse HOM dip, and obtain larger entanglement entropy compared with regular CROWs. We present conclusions and an outlook in Section 5.

2. MODEL OF H-CROWS WITH DISORDER-ROBUST TRANSPORT

The helical-CROW (H-CROW) consists of two legs of resonant ring cavities coupled via off-resonant link rings, as illustrated in Fig. 2. We assume decoupled circulation modes of each cavity, which allows one to effectively break time-reversal symmetry by making the link rings asymmetric. We are interested in the propagation of wave packets close to the band center, where the tight-binding approximation is valid [24,35].

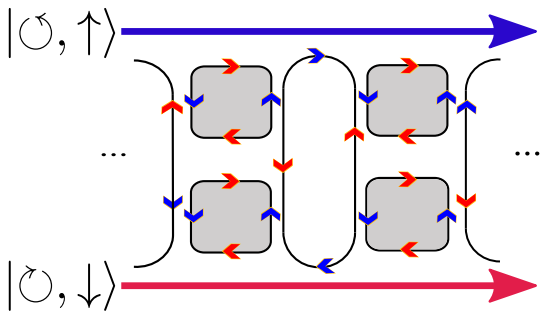

Fig. 2. Schematic of the helical coupled-resonator optical waveguide (H-CROW). Pseudospin-momentum locking is achieved after a certain propagation distance, where each sublattice exhibits definite momentum for designated circulation mode, thereby facilitating a disorder-resistant transport. As opposite circulations exhibit opposite helicity, two co-propagating channels can be realized.

Under this approximation, each unit cell hosts two sites, with coupling between nearest and next-nearest neighbors.

The tight-binding Hamiltonian governing time evolution of one specific circulation direction (counterclockwise) in the absence of disorder reads [24,25,33,36]

$$\begin{aligned}\hat{H}_{0,\mathrm{ccw}} &= \sum_n (\hat{H}_{a,\mathrm{ccw}} + \hat{H}_{b,\mathrm{ccw}} + \hat{H}_{ab,\mathrm{ccw}} + \hat{H}^{\dagger}_{ab,\mathrm{ccw}}),\\ \hat{H}_{a,\mathrm{ccw}} &= J\hat{a}^{\dagger}_n(-i\hat{a}_{n-1} + i\hat{a}_{n+1}),\\ \hat{H}_{b,\mathrm{ccw}} &= J\hat{b}^{\dagger}_n(i\hat{b}_{n-1} - i\hat{b}_{n+1}),\\ \hat{H}_{ab,\mathrm{ccw}} &= 2J\hat{a}^{\dagger}_n\left[\hat{b}_n + \frac{1}{2}(\hat{b}_{n-1} + \hat{b}_{n+1})\right],\end{aligned} \tag{1}$$

where J is the hopping strength, and field operators $\hat{a}_n, \hat{b}_n$ represent the annihilation operators at the sites in the nth unit cell, while their conjugates are associated with the corresponding creation operators. The complex hopping terms arise due to the specially introduced asymmetry of the link rings [33]. Note that we measure frequencies with respect to a resonance of a single isolated ring, such that the eigenvalues of $\hat{H}_{\mathrm{ccw}}$ are modal frequency detunings with respect to this resonance.

Let us now consider a periodic lattice, which enables us to compactly write the Hamiltonian in k-space as

$$\hat{H}_{0,\mathrm{ccw}} = \sum_k \psi^{\dagger}_{k,\mathrm{ccw}}[\boldsymbol{d}(k)\cdot\hat{\boldsymbol{\sigma}}]\psi_{k,\mathrm{ccw}}, \tag{2}$$

where k is the crystal momentum, $\psi_{k,\mathrm{ccw}} = (\hat{a}_{k,\mathrm{ccw}}, \hat{b}_{k,\mathrm{ccw}})^T$, $\boldsymbol{d} = (d_0, d_x, d_y, d_z) = (0, 2J(1+\cos k), 0, -2J\sin k)$, $\hat{\boldsymbol{\sigma}}$ are Pauli matrices, and we now interpret the upper ($\hat{a}$) and lower ($\hat{b}$) layers as corresponding to up and down pseudospin degrees of freedom, respectively. The eigenvalues of $\hat{H}_{\mathrm{ccw}}$ are $\omega_{\pm}(k) = \pm 2\sqrt{2}J\sqrt{1+\cos k}$. The first component, d_0, describes the symmetric part of the intra-leg coupling, which vanishes under our choice of hopping phase [33], $2J\hat{\sigma}_x$ is analogous to a Zeeman field, and $2J\cos k\hat{\sigma}_x$ and $-2J\sin k\hat{\sigma}_z$ resemble intrinsic and Rashba-like spin-orbit couplings, respectively.

For the opposite excitation (clockwise), propagation is governed by the time-reversed Hamiltonian $\hat{H}_{\mathrm{cw}}$, which exhibits opposite hopping phases due to time-reversal symmetry [37]. We introduce a total Hamiltonian composed of both

circulations given in the direct product form, $\hat{H}_{\rm tot} = \hat{H}_{\rm ccw} \oplus \hat{H}_{\rm cw}$. We obtain pseudospin-momentum locking in the center of the passband ($k = \pi$), where $\omega = 0$, $d_x = 0$, and the wave group velocity becomes $d\omega_{\pm}/dk = \pm 2J$. It supports the most resistant light propagation against disorder, since $\mathcal{H}_{\rm tot}(k)$ for the small momentum deviations $k = \pi + \Delta k$ has the form

$$\mathcal{H}_{\rm tot}(\pi + \Delta k) \approx 2J\,\mathrm{diag}(\Delta k, -\Delta k, -\Delta k, \Delta k), \tag{3}$$

where Eq. (3) is written in the basis $\{|\circlearrowleft,\uparrow\rangle, |\circlearrowleft,\downarrow\rangle, |\circlearrowright,\uparrow\rangle, |\circlearrowright,\downarrow\rangle\}$; the first index labels the circulation direction, and the second indicates the pseudospins. Note that the off-diagonal component describing pseudospin-flipping vanishes in the first (linear) order of deviation.

At the band center, H-CROWs show the maximum Anderson localization length and most resistant temporal pulse propagation, since the most significant disorder is misalignment of the rings' resonant frequencies, which is diagonal in the sublattice basis and does not flip the pseudospin [12,16,25,26,33,38].

Importantly, we can employ the circulation degree of freedom to use H-CROWs as two-mode delay lines (see Fig. 2). By exciting both circulations through different sublattices, the simultaneous pseudospin-momentum locking phases (red and blue) can be obtained. We now consider the propagation of light in the presence of disorder and losses. For the sake of simplicity, we only take the dominant on-site disorder into account, which has the form [33]

$$\hat{V}_{\epsilon} = \sum_{n} (V^{(a)}_{n,\epsilon} \hat{a}^{\dagger}_{n} \hat{a}_{n} + V^{(b)}_{n,\epsilon} \hat{b}^{\dagger}_{n} \hat{b}_{n}), \tag{4}$$

where ϵ labels each disorder realization. We assume that each on-site potential $V^{(j)}_{n,\epsilon}$ has a Gaussian distribution with mean zero and standard deviation U.

We first formulate equations for the field operators $\hat{\psi}_n = (\hat{a}_n, \hat{b}_n)^T$ to calculate the transmission at a given frequency ω; the equation reads [25,39]

$$\begin{aligned} i\omega\hat{\psi}_{n,j}(\omega) = {} & i[\hat{H}_{0,j}, \hat{\psi}_{n,j}(\omega)] - \kappa_{\rm ex}\hat{\psi}_{n,j}(\omega)(\delta_{n,1} + \delta_{n,L}) \\ & - \kappa_{\rm in}\hat{\psi}_{n,j}(\omega) + \sqrt{2\kappa_{\rm ex}}\,\hat{p}_{{\rm in},j}(\omega)\delta_{n,1}, \end{aligned} \tag{5}$$

where $j = 1$ (ccw) and $j = 2$ (cw) index counterclockwise and clockwise circulation modes, respectively, $\kappa_{\rm in}$ is the intrinsic scattering losses of each cavity, $\kappa_{\rm ex}$ is coupling strength to the input/output leads at each edge of the array, and L is the array length. The input field entering the first unit cell is $p_{\rm in}(\omega)$, and we assume wave packets with identical temporal distributions but opposite circulations and sublattices, which excite the two helical modes.

The reflection (R) and transmission (T) amplitudes can be expressed for the two inputs as follows [24,25]:

$$\begin{aligned} R_1(\omega) &= \left| \frac{p_{\rm in}(\omega) - \sqrt{2\kappa_{\rm ex}} a_1(\omega)}{p_{\rm in}(\omega)} \right|^2, \\ T_1(\omega) &= \left| \frac{\sqrt{2\kappa_{\rm ex}} a_L(\omega)}{p_{\rm in}(\omega)} \right|^2, \\ R_2(\omega) &= \left| \frac{p_{\rm in}(\omega) - \sqrt{2\kappa_{\rm ex}} b_1(\omega)}{p_{\rm in}(\omega)} \right|^2, \\ T_2(\omega) &= \left| \frac{\sqrt{2\kappa_{\rm ex}} b_L(\omega)}{p_{\rm in}(\omega)} \right|^2, \end{aligned} \tag{6}$$

where operators without a "hat" refer to their corresponding field components of sublattices a, b [40]. The derivation is given in Appendix A. We note the following relation for the output field operators [39]:

$$\hat{p}_{\rm out,1} = -\sqrt{2\kappa_{\rm ex}}\hat{a}_L, \qquad \hat{p}_{\rm out,2} = -\sqrt{2\kappa_{\rm ex}}\hat{b}_L. \tag{7}$$

Given the transmission spectrum, we can compute the wave packets' group delay times τ_j via

$$\tau_j = \frac{1}{i}\frac{\mathrm{d}}{\mathrm{d}\omega}\left[\frac{p_{{\rm out},j}(\omega)}{|p_{{\rm out},j}(\omega)|}\right] \qquad (j = 1, 2), \tag{8}$$

where $p_{\rm out,j}(\omega)$ refers to the corresponding field component. This quantity measures the transit time of a wave packet through the device. The distribution of delay times provides a measure of the sensitivity of the system to disorder [26].

We present in Fig. 3(a) intensity profiles in the first half of an $L = 20$ H-CROW for a monochromatic input at $\omega = 0$ (the middle of the transmission band), averaged over an ensemble of 500 disorder realizations. For comparison, Fig. 3(b) shows the intensity profile of a regular CROW. The numerical calculations are performed using parameters similar to the experiments in Refs. [25,26]: $\kappa_{\rm ex} = 0.5J$, $\kappa_{\rm in} = 0.1J$, and disorder standard deviation $U = 0.8J$. In physical units, this corresponds to an operating wavelength $\lambda \approx 1550$ nm, with $\kappa_{\rm ex} \sim 15$ GHz, $\kappa_{\rm in} \sim 2$ GHz, and hopping strength $J \sim 30$ GHz [25,26]. In the H-CROW, the intensity remains confined to the upper (a) sublattice, signifying pseudospin-momentum locking, with the attenuation of the intensity along the array occurring only due to the internal losses $\kappa_{\rm in}$. The regular CROW also exhibits Anderson localization, resulting in more rapid attenuation of the intensity in Fig. 3(b).

We plot in Fig. 3(c) the transmission spectra in Eq. (6), where the shaded regions indicate the 65% confidence intervals [25]. H-CROWs achieve higher transmission than regular CROWs through the entire passband, with almost five times higher transmission at $\omega = 0$ and smaller deviations between different disorder realizations as a result of the disorder resistant unidirectional propagation. Figure 3(d) demonstrates that H-CROWs maintain the amplitude of the output field for a broad range of disorder strengths U, while CROWs show increasingly poor performance as U increases. Based on these results, we use $U = 0.8J$ as a disorder strength in the following, as this regime clearly illustrates the advantage of H-CROWs versus regular CROWs in the presence of the moderate disorder typically present in experiments [24]. We note that the comparatively lower transmission of the H-CROW for weak disorder is due to nonoptimal input coupling, which can be

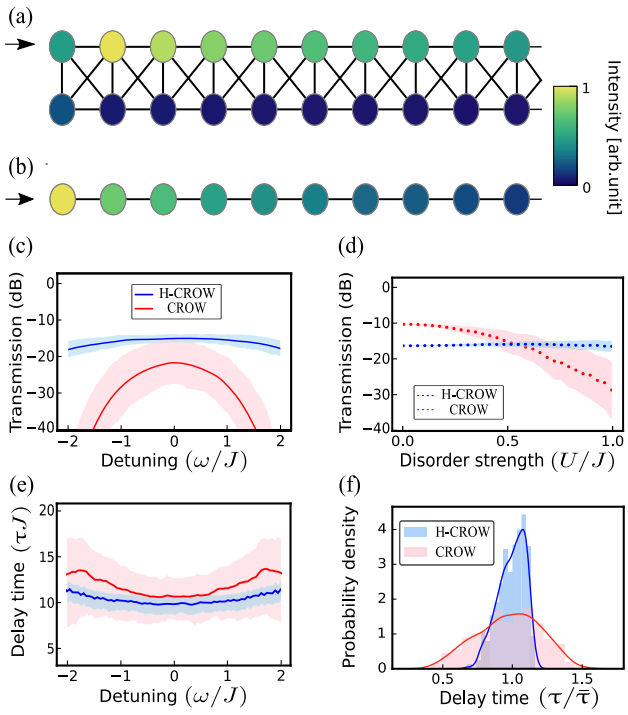

Fig. 3. Classical wave transport through H-CROWs and CROWs in the presence of moderate disorder $U = 0.8J$ and intrinsic losses $\kappa_{in} = 0.1J$. (a), (b) Disorder-averaged field intensity profiles at $\omega = 0$ in the first 10 rings of an $L = 20$ (a) H-CROW and (b) CROW. (c) Frequency-dependent transmission spectra. Solid lines indicate the disorder average; shaded regions represent 65% confidence interval. Maximum of average is −15.8 and −22.8 dB at $\omega = 0$ for the H-CROW and CROW, respectively. (d) Dependence of the transmission at $\omega = 0$ on the disorder strength U. (e) Wave packet delay time as a function of the input frequency. (f) Distribution of delay times at $\omega = 0$, where $\bar{\tau}$ is the root mean square delay.

improved by, e.g., coupling the input waveguide to the second unit cell of the array.

The effects of disorder on the group delay time versus frequency detuning are presented in Fig. 3(e). We see that H-CROWs exhibit a slightly smaller average delay but much lower fluctuations. Furthermore, the statistics of delay times in the vicinity of $\omega = 0$ presented in Fig. 3(f) show that H-CROWs exhibit more ballistic transport than regular CROWs; as for H-CROWs, the delay time distribution around the root mean square average has a Gaussian shape with smaller variance.

3. PRESERVATION OF PHOTON INDISTINGUISHABILITY

In this section, we consider the transmission of two identical photons forming a separable quantum state at the input and analyze the degree of temporal photon indistinguishability at the output of the H-CROW and CROW. Specifically, we consider an input state $|11\rangle_{cw,ccw}$, with one photon in the clockwise mode and a temporally identical photon in the counterclockwise mode. The output state in the frequency domain has the form

$$|\text{out}\rangle = \hat{\phi}_a\hat{\phi}_b|00\rangle_{ab} = \int d\omega \int d\omega' p_{\text{out},1}(\omega)p_{\text{out},2}(\omega')\hat{a}^\dagger_{\text{out}}(\omega)\hat{b}^\dagger_{\text{out}}(\omega')|00\rangle_{ab}, \tag{9}$$

where the subscripts a and b indicate the Hilbert space corresponding to upper/lower part of output port with the field operators $\hat{\phi}_{a/b} := \int d\omega \hat{p}_{\text{out},1/2}(\omega)$ composed of field creation operators of each output port $\hat{a}^\dagger_{\text{out}}$, $\hat{b}^\dagger_{\text{out}}$. Note that we are working with scalar fields, assuming a fixed polarization state.

We compare a degree of the temporal overlap of the two photons after each one propagates through a different part of the device by calculating the coincidence probability. It was the first experimental witness of quantum property, as Hong *et al.* showed quantumness by generating entangled photons and measuring their coincidence counts versus the controlled delay to one of the paths [34]. When the total time delay is zero, coincidence rates after a 50:50 beam splitter reach a minimum and vanish due to the quantum interference when photons are temporally indistinguishable. Accordingly, we analyze the photon interference at the output with a tunable temporal delay, as illustrated in Figs. 4(a) and 4(b). When a two-photon output state passes a beam splitter with ratio $r:t$, where r and t represent reflection and transmission, respectively, the field operators obey the unitary relation [41]

$$\begin{pmatrix} \hat{c}^\dagger \\ \hat{d}^\dagger \end{pmatrix} = \begin{pmatrix} t & ir \\ ir & t \end{pmatrix} \begin{pmatrix} \hat{a}^\dagger_{\text{out}} \\ \hat{b}^\dagger_{\text{out}} \end{pmatrix}, \tag{10}$$

where $t^2 + r^2 = 1$ $(t, r \in \mathcal{R})$ and $\hat{c}, \hat{d}$ indicate the field operators of upper/lower sides after passing the beam splitter. We calculate the coincidence probability of the simultaneous "clicks" with the two single-photon detectors, P_{coin}, using the projection operator $\hat{P}_c \otimes \hat{P}_d := \int d\omega \hat{c}^\dagger(\omega)|0\rangle\langle 0|\hat{c}(\omega) \otimes \int d\omega' \hat{d}^\dagger(\omega')|0\rangle\langle 0|\hat{d}(\omega')$ [42]. Thus, $P_{\text{coin}} = \text{Tr}[\rho \hat{P}_c \otimes \hat{P}_d]$, where the density matrix is $\rho = |\text{out}\rangle\langle\text{out}|$. Now, we introduce a tunable delay parameter between two outputs τ_c, which controls the temporal overlap between the photons before their interference on the beam splitter. Without loss of generality, we apply this delay to the lower output port and obtain a final expression for a balanced beam splitter $(t = r = 1/\sqrt{2})$ [43]:

$$P_{\text{coin}}(\tau_c) = \frac{1}{2}\left[1 - \frac{|\int d\omega p_1^*(\omega)p_2(\omega)e^{i\omega\tau_c}|^2}{\int d\omega |p_1(\omega)|^2 \int d\omega' |p_2(\omega')|^2}\right]. \tag{11}$$

The second part of the above equation defines the visibility V, $V = \sqrt{1 - 2P_{\text{coin}}}$ [41], which quantifies the degree of interference. In quantum mechanics, it is also referred to as indistinguishability of photons [44]. The meaning of coincidence probability is thus the resultant distribution of indistinguishability [45]. Note that coincidence probability is zero for an ideal case of identical single photons, indicating indistinguishability preservation, since the transformation for the indistinguishable photon input state reads [46,47]

$$|11\rangle_{ab} \to \frac{1}{\sqrt{2}}(|20\rangle_{ab} + |02\rangle_{ab}). \tag{12}$$

Conversely, for a very large time delay exceeding the wave packet temporal width, the photons do not interfere with each other, and the coincidence probability becomes 1/2 for a balanced

(50:50) beam splitter, corresponding to distinguishable photons according to the calculations in Appendix B.

We perform a comparison against regular CROWs with the same input and same propagation length, as illustrated in Figs. 4(a) and 4(b). We consider wave packets with a Gaussian envelope at the input, i.e., $p_{\text{in}}(\omega) = \exp(-\omega^2/2\sigma^2)$, where $\sigma = 0.5J$ is the envelope width. We plot in Fig. 4(c) the calculated coincidence probability versus controlled time delay after propagation through the 20-ring CROW, as discussed above. We note that the separable two-photon state is insensitive to the relative phase delay accumulated along the different paths, as sketched in Fig. 1(a), but can be affected by disorder-induced variations in the group delay and wave packet distortions, as indicated in Figs. 1(b) and 1(c). We observe that the minimum coincidence probability for H-CROWs remains close to zero ($\approx 2 \times 10^{-4}$), indicating photon indistinguishability is well-preserved. On the contrary, for regular CROWs, the mean minimum coincidence probability is 0.22, which means that photons become partially distinguishable due to disorder. Even though the two photons with opposite spins travel along different disordered paths, the temporal shape of photons at the H-CROW outputs remains almost identical or indistinguishable, as a result of disorder-resistant transport. This advantage becomes more pronounced for longer CROWs, as shown in Fig. 4(d). The minimum coincidence for H-CROWs remains small ($\lesssim 4 \times 10^{-3}$), whereas the minimum coincidence probability for the regular CROWs keeps increasing, indicating reduced indistinguishability as the length of the delay line increases.

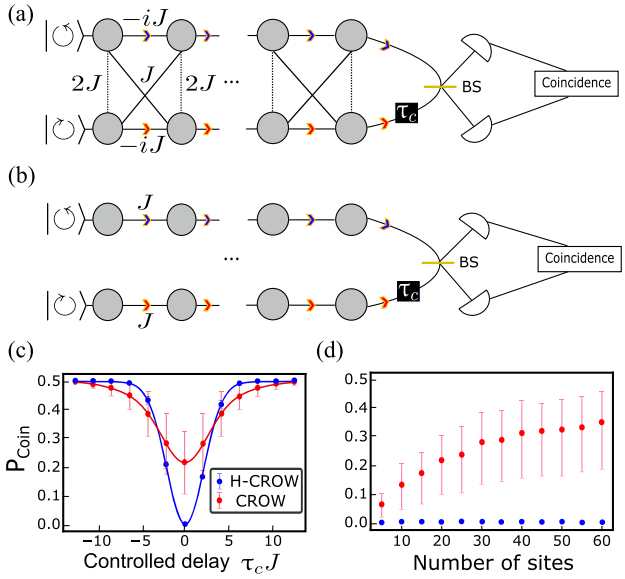

Fig. 4. (a), (b) Schematics of coincidence measurement using tight-binding models of an H-CROW and a pair of regular CROWs. We consider measurements for two photons exhibiting opposite helicity with controlled delay time τ_c before a 50:50 beam splitter (BS) and resulting coincidence probability of two photons to produce simultaneous "clicks" of single-photon detectors. (c) Coincidence versus controlled delay time for 20-site long CROW structures. (d) Minimum coincidence values with respect to the number of sites. Blue solid line and dots represent the average for H-CROWs and red for CROWs. Error bars indicate 65% confidence interval for 500 disorder realizations.

4. PROTECTION OF PHOTON ENTANGLEMENT

We now aim to show that H-CROWs can preserve a peculiar quantum property of transmitted photons, entanglement inherently originating from the quantum coherence. Let us consider an N00N state as an input, $|N::N\rangle := (|N0\rangle + |0N\rangle)/\sqrt{2}$. Hereafter we omit the 'ab' notation. Such states are strongly sensitive to all effects of the disorder, as sketched in Fig. 1, including phase fluctuations [48], in contrast with the separable states we analyzed in the previous section. The corresponding output state in the frequency domain $|\text{out}\rangle$ is

$$\begin{aligned}|\text{out}\rangle &= \frac{1}{\sqrt{2}\sqrt{N!}}(\hat{\phi}_a^N + \hat{\phi}_b^N)|00\rangle \\ &= \frac{1}{\sqrt{2N!}}\left[\int \prod_{i=1}^{N} \mathrm{d}\omega_i p_1(\omega_i)\hat{a}_{\text{out}}^\dagger(\omega_i)\right. \\ &\quad \left. + \int \prod_{i=1}^{N} \mathrm{d}\omega_i p_2(\omega_i)\hat{b}_{\text{out}}^\dagger(\omega_i)\right]|00\rangle, \end{aligned} \tag{13}$$

where $\hat{\phi}_j$ are the output field operators introduced in the previous section. Let us consider the two-photon state with $N = 2$, which can be simply created from a separable state by passing it through a balanced beam splitter before coupling into the CROW. The output state, after applying the time delay (τ_c) but before the very last interference stage, can be expressed as

$$\begin{aligned}|\text{out}(\tau_c)\rangle_{\text{bef}} &= \frac{1}{2}\int \mathrm{d}\omega_1 \mathrm{d}\omega_2 [p_1(\omega_1)p_1(\omega_2)\hat{a}_{\text{out}}^\dagger(\omega_1)\hat{a}_{\text{out}}^\dagger(\omega_2) \\ &\quad + p_2(\omega_1)p_2(\omega_2)\hat{b}_{\text{out}}^\dagger(\omega_1)\hat{b}_{\text{out}}^\dagger(\omega_2)e^{i(\omega_1+\omega_2)\tau_c}]|00\rangle. \end{aligned} \tag{14}$$

We first analyze the case of indistinguishable photons at the output and note that, in this ideal situation, the disorder can introduce a phase difference θ between the photons in two output ports. The transformation of such a state by output of a 50:50 beam splitter implements a reversed Hong–Ou–Mandel (HOM) interference [49], which we express as follows:

$$\begin{aligned}&\frac{1}{\sqrt{2}}(|20\rangle + e^{i\theta}|02\rangle) \\ &\rightarrow \frac{1}{2\sqrt{2}}[(1 - e^{i\theta})|20\rangle + \sqrt{2}i(1 + e^{i\theta})|11\rangle - (1 - e^{i\theta})|02\rangle]. \end{aligned} \tag{15}$$

The coincidence probability is then

$$P_{\text{coin}} = \frac{1 + \cos\theta}{2}. \tag{16}$$

Note that the coincidence probability can oscillate, even though the entangled state remains pure. This is due to the phase sensitivity of the N00N state [50].

Next, we determine the coincidence probability in the general case, considering all the effects due to disorder. We compute the density matrix of the output state $\rho = |\text{out}\rangle\langle\text{out}|$ using the projection operators

$$|20\rangle\langle 20| = \frac{1}{2}\int d\omega_1 d\omega_2 \hat{a}^\dagger_{\text{out}}(\omega_1)\hat{a}^\dagger_{\text{out}}(\omega_2)|00\rangle\langle 00|\hat{a}_{\text{out}}(\omega_2)\hat{a}_{\text{out}}(\omega_1),$$

$$|02\rangle\langle 02| = \frac{1}{2}\int d\omega_1 d\omega_2 \hat{b}^\dagger_{\text{out}}(\omega_1)\hat{b}^\dagger_{\text{out}}(\omega_2)|00\rangle\langle 00|\hat{b}_{\text{out}}(\omega_2)\hat{b}_{\text{out}}(\omega_1),$$

$$|11\rangle\langle 11| = \int d\omega_1 d\omega_2 \hat{a}^\dagger_{\text{out}}(\omega_1)\hat{b}^\dagger_{\text{out}}(\omega_2)|00\rangle\langle 00|\hat{b}_{\text{out}}(\omega_2)\hat{a}_{\text{out}}(\omega_1), \quad (17)$$

respectively. Again, $\hat{a}_{\text{out}}, \hat{b}_{\text{out}}$ denote annihilation operators on upper and lower output legs, respectively. The coincidence probability with the normalized output $\text{Tr}[\rho] = 1$ is given by

$$P_{\text{coin}}(\tau_c) = \frac{1}{2}\left\{1 + \frac{[\int d\omega p_1^*(\omega)p_2(\omega)e^{i\omega\tau_c}]^2 + \text{c.c.}}{[\int d\omega|p_1(\omega)|^2]^2 + [\int d\omega|p_2(\omega)|^2]^2}\right\}. \quad (18)$$

In agreement with the expression written in Fock basis in Eq. (16), here phase fluctuations θ arise from phase mismatches between the fields $p_{1,2}(\omega)$. Note that the coincidence probability is $\langle 11|\rho|11\rangle$, which we derive in Appendix C.

To quantify the mixture of the output state induced by disorder, we also analyze another quantity, the purity $\text{Tr}[\rho^2]$, which is bounded by $1/d \le \text{Tr}[\rho^2] \le 1$, where d is the dimension of Hilbert space, i.e., $d = 2$ for the two-photon case. The maximum value corresponds to pure states and the minimum to fully mixed states. The state purity after passing the controlled delay is

$$\text{Tr}[\rho^2(\tau_c)] = 1 + 2\left\{\frac{(|\int d\omega p_1^* p_2 e^{i\omega\tau_c}|^2)^2 - (\int d\omega|p_1|^2 \int d\omega'|p_2|^2)^2}{[(\int d\omega|p_1|^2)^2 + (\int d\omega|p_2|^2)^2]^2}\right\}, \quad (19)$$

where we omit the integral variable ω, ω' to simplify notation.

The form of Eq. (19) reveals that the output state remains pure when indistinguishability is preserved. Namely, since we consider noninteracting particles, we can relate the N00N state purity to the coincidence probability of the separable input state $|11\rangle_{ab}$, according to Eq. (11). Since $P_{\text{coin}}(\tau_c) \approx 0$, we have $|\int d\omega p_1^* p_2 e^{i\omega\tau_c}|^2 \approx (\int d\omega|p_1|^2)(\int d\omega'|p_2|^2)$, indicating that the two output fields p_1, p_2 have identical intensities and group delays. The expression in Eq. (19) thereby approaches 1, even though coincidence probability for $|2::2\rangle$ may fluctuate due to the phase sensitivity of N00N state.

To verify this reasoning, we plot in Figs. 5(a) and 5(b) the distributions of coincidence probability for N00N states transmitted through H-CROWs and regular CROWs, respectively, with a zero-controlled time delay ($\tau_c = 0$). We observe that, for H-CROWs, the oscillation of probability occurs in the full range of [0,1], which is evidence that entanglement is preserved. In contrast, the coincidences from the regular CROWs show a peak at 0.5, indicating the output state is mixed and the entanglement is lost due to disorder.

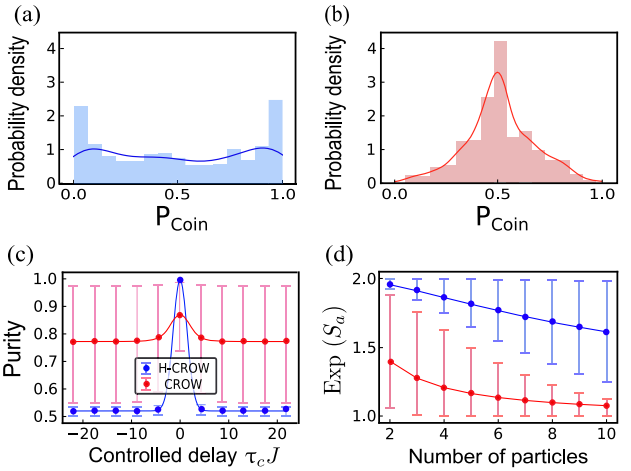

Fig. 5. Disorder-robust transmission of $N = 2$ N00N states using the H-CROW. (a), (b) Statistics of the output coincidence probability for the (a) H-CROW and (b) regular CROWs. (c) Output state purity versus controlled delay time for the H-CROW (blue) and regular CROW (red), with error bars indicating 65% confidence interval. (d) Exponentiated entanglement entropy of the upper output port, $\exp(S_a)$, as a function of the photon number N. $\exp(S_a)$ distinguishes maximally entangled states $\exp(S_a) = 2$ from separable states $\exp(S_a) = 1$. We use an ensemble of 500 disorder realizations and disorder strength $U = 0.8J$.

We additionally show in Fig. 5(c) the average purity and the 65% confidence interval versus the delay time. We see that purity stays at 1 for H-CROWs at zero delay, while CROWs exhibit loss of coherence with huge fluctuations due to disorder. As the delay is increased, entangled photons in H-CROW become a completely mixed state with purity 0.5, as their coherence is washed out. On the other hand, in the regular CROW the average purity remains higher but with large fluctuations. This is because the transmission amplitude is sensitive to the disorder. Suppose we obtain the much higher transmission through one leg compared with the other. Then, according to Eq. (19), the temporal purity will be unity regardless of controlled delay. In addition, large group delay fluctuation in CROWs also affects the distribution of purity. For instance, even though we apply time delay to one of the waveguides, packets can be detected at the same moment due to the group delay induced by disorder.

To further quantify the effect of disorder, we consider the entanglement entropy S_a, which indicates the capacity for encoding quantum information [51],

$$S_a := -\text{Tr}_a[\rho_a \ln(\rho_a)], \quad (20)$$

where $\rho_a = \text{Tr}_b[\rho(\tau_c)]$. Note that, as coherence terms vanish by partial trace, the controlled delay does not affect the entropy. We compute the entanglement entropy in Appendix C,

$$S_a = -x\ln x - (1-x)\ln(1-x), \quad (21)$$

where for the two-photon ($N = 2$) N00N state we have

$$x = \frac{[\int d\omega|p_{\text{out},1}(\omega)|^2]^2}{[\int d\omega|p_{\text{out},1}(\omega)|^2]^2 + [\int d\omega|p_{\text{out},2}(\omega)|^2]^2}. \quad (22)$$

The entanglement is maximized when $x = 0.5$, corresponding to identical intensities at the two output ports. This demonstrates

the higher capacity of H-CROWs, which exhibit almost identical output intensities from the upper and lower ports. In contrast, CROWs yield poor capacity as the intensity ratio differs due to disorder.

We show in Fig. 5(d) the scaling of the entanglement entropy with the number of photons, revealing huge fluctuations and loss of entanglement for the regular CROW, while the H-CROW can preserve some amount of entanglement. As we increase N, we observe larger fluctuations of the entanglement entropy. The entangled photons in the regular CROW become a mixed state due to the large transmission fluctuations, i.e., appreciable transmission only occurs along one leg. Thus, entanglement entropy becomes 0 and the error bar of entanglement entropy becomes smaller. We emphasize that, for a given delay or N, the H-CROW exhibits better performance of protecting entanglement than the regular CROW. One caveat on entanglement entropy is that it is not sensitive to the controlled delay time, as it only depends on the intensity at each output port. To obtain the maximum entanglement entropy, the intensity at each output port should be identical, which can be seen from Eq. (22).

5. CONCLUSION

In this paper, we have studied the propagation of quantum states of light through helical coupled-resonator waveguides (H-CROWs). Regular CROWs can serve as delay lines in integrated photonic circuits; however, they exhibit strong sensitivity to fabrication disorder preventing reliable transmission of wave packets. H-CROWs exploit an additional sublattice degree of freedom to achieve disorder-resistant transport, which arises due to one-way modes at the center of their transmission band, whose propagation direction is fixed by the excited sublattice (known as pseudospin-momentum locking). Using numerical solutions of tight-binding models describing H-CROWs and regular CROWs, we have shown that the former can be used to more reliably transport quantum states of light in the presence of disorder.

We first showed that transmission probability and wave packet delay times have narrower fluctuations and provide more ballistic-like transport compared with regular CROWs. Next, we showed that two identical photons transmitted through an H-CROW can preserve the indistinguishability of their temporal wave packets and, accordingly, demonstrate the quantum Hong–Ou–Mandel interference. Finally, we showed that path-entangled two-photon N00N states are preserved as pure entangled states, while the effect of disorder is only expressed through the accumulation of a relative phase between the photon pairs. We note that this relative phase fluctuation can be compensated by simply placing a single tunable phase shifter at one of the output ports [38]. The H-CROWs perform better at reliably transporting both types of quantum states, while quantum features are strongly suppressed by disorder in regular CROWs.

In the future, it will be interesting to generalize our findings to multimode entangled states and multimode H-CROWs. Moreover, in this work we considered weakly coupled resonators described by the tight binding approximation, similar to the experiments in Refs. [25,26]. In order to increase the operating bandwidth, it would be essential to consider more strongly coupled lattices, which must be modeled using the transfer matrix method [33]. We expect that our results can provide a practical way to create robust integrated photonic delay lines, which can serve as essential components facilitating reliable generation and guiding of the quantum state of light for multiple applications, including scalable quantum information processing.

APPENDIX A. INPUT–OUTPUT RELATION

When we induce the coupling between an external probe waveguide characterized by field operator $\hat{p}$ and the system, the dynamics are governed by total Hamiltonian,

$$\hat{H}_{\text{tot}} = \hat{H}_{\text{sys}} + \hat{H}_{\text{env}} + \hat{H}_{\text{int}}, \tag{A1}$$

where $\hat{H}_{\text{sys}}$ is our Hamiltonian of interest. Hamiltonians describing the environment $\hat{H}_{\text{env}}$ and the interaction between system and environment $\hat{H}_{\text{int}}$ are given by

$$\begin{aligned}\hat{H}_{\text{env}} &= \int_{-\infty}^{\infty} \mathrm{d}\omega\, \omega \hat{p}^{\dagger}(\omega, t)\hat{p}(\omega, t),\\ \hat{H}_{\text{int}} &= i\int_{-\infty}^{\infty} \mathrm{d}\omega \sqrt{2\kappa_{\text{ex}}}[\hat{a}^{\dagger}(t)\hat{p}(\omega, t) - \text{h.c.}],\end{aligned} \tag{A2}$$

where κ_{ex} is an external coupling parameter independent of frequency, $\hat{a}$ is the coupling field operator of system, e.g., $\hat{a}_1$ for upper input port. Note that $\hat{p}_{\text{in}}$ lives in a different Hilbert space from the resonator field operators $\hat{a}_j$, as it represents the field operator of environment. Besides, negative frequencies are allowed, as we work in a rotating frame at a frequency much larger than typical bandwidths we consider [39]. Here, we assume that the probe waveguide has an almost continuous spectrum. The Heisenberg equation of the bath operator reads [39]

$$\frac{\mathrm{d}}{\mathrm{d}t}\hat{p}(\omega, t) = -i\omega\hat{p}(\omega, t) - \sqrt{2\kappa_{\text{ex}}}\hat{a}(t). \tag{A3}$$

The solution of the above is

$$\hat{p}(\omega, t) = e^{-i\omega(t-t_0)}\hat{p}(\omega, t_0) - \sqrt{2\kappa_{\text{ex}}}\int_{t_0}^{t} \mathrm{d}t' e^{-i\omega(t-t')}\hat{a}(t'), \tag{A4}$$

where t_0 is the initial time. Here, the input field $\hat{p}_{\text{in}}(t)$ is defined as [39]

$$\hat{p}_{\text{in}}(t) := \frac{1}{\sqrt{2\pi}}\int_{-\infty}^{\infty} \mathrm{d}\omega e^{-i\omega(t-t_0)}\hat{p}(\omega, t_0) \qquad (t > t_0), \tag{A5}$$

which is a Fourier transform of the input spectrum. Then, Eq. (A4) can be written differently:

$$\begin{aligned}\int \mathrm{d}\omega\hat{p}(\omega, t) &= \hat{p}_{\text{in}}(t) - \sqrt{2\kappa_{\text{ex}}}\int_{-\infty}^{\infty} \mathrm{d}\omega \int_{t_0}^{t} \mathrm{d}t' e^{-i\omega(t-t')}\hat{a}(t')\\ &= \hat{p}_{\text{in}}(t) - \frac{\sqrt{2\kappa_{\text{ex}}}}{2}\hat{a}(t),\end{aligned} \tag{A6}$$

where we use $\Theta(t) := \int_{-\infty}^{t} \mathrm{d}t'\delta(t')$, and $\Theta(0) = 1/2$. We can introduce another solution by defining final time t_1, which yields the solution

$$\hat{p}(\omega,t)=e^{-i\omega(t-t_1)}\hat{p}(\omega,t_1)-\sqrt{2\kappa_{ex}}\int_{t_1}^{t}dt'e^{-i\omega(t-t')}\hat{a}(t'). \tag{A7}$$

Let us define output field operator $\hat{p}_{out}$, where

$$\hat{p}_{out}(t):=\frac{1}{\sqrt{2\pi}}\int d\omega e^{-i\omega(t-t_1)}\hat{p}(\omega,t_1)\qquad (t<t_1), \tag{A8}$$

which yields

$$\begin{aligned}\int d\omega\hat{p}(\omega,t)&=\hat{p}_{out}+\sqrt{2\kappa_{ex}}\int_{-\infty}^{\infty}d\omega\int_{t}^{t_1}dt'e^{-i\omega(t-t')}\hat{a}(t')\\&=\hat{p}_{out}(t)+\frac{\sqrt{2\kappa_{ex}}}{2}\hat{a}(t).\end{aligned} \tag{A9}$$

We can hence find the identity between input and output [39]:

$$\hat{p}_{in}(t)-\hat{p}_{out}(t)=\sqrt{2\kappa_{ex}}\hat{a}(t), \tag{A10}$$

which yields the representations of reflection and transmission coefficients described in Eq. (6).

APPENDIX B. COINCIDENCE PROBABILITY FOR GENERAL BEAM SPLITTER

Suppose identical photons come toward a beam splitter (BS) from the opposite ports as depicted in Figs. 4(a) and 4(b). The BS exhibits the ratio $r:t$, where r, $t(\in\mathcal{R})$ are the reflectivity and transmissivity, respectively, $r^2+t^2=1$. The transformation for indistinguishable photons reads [46,47]

$$|11\rangle_{ab}\to irt\sqrt{2}|20\rangle_{ab}+irt\sqrt{2}|02\rangle_{ab}+(t^2-r^2)|11\rangle_{ab}, \tag{B1}$$

where modes a and b indicate the photons coming from upper and lower parts, respectively. The coincidence probability is now given by $P_{coin}=(t^2-r^2)^2$. Minimum coincidence occurs when $r=t=1/\sqrt{2}$, yielding 0 coincidence. On the other hand, given two photons are distinguishable, Eq. (B1) is then

$$\begin{aligned}|1001\rangle_{a_1b_1a_2b_2}\to{}&irt|1010\rangle_{a_1b_1a_2b_2}+irt|0101\rangle_{a_1b_1a_2b_2}\\&+t^2|1001\rangle_{a_1b_1a_2b_2}-r^2|0110\rangle_{a_1b_1a_2b_2},\end{aligned} \tag{B2}$$

and it turns out that the coincidence probability of measuring photons on each detector simultaneously is $P_{coin}=t^4+r^4$. Then, 0.5 is the lowest value possible for a classical field when the splitting ratio is 50:50. Hence, $P_{coin}=0.5$ implies the boundary between quantum and classical cases, where a lower value is only possible due to quantum interference between (partially) indistinguishable photons [41,47,52].

Similar to our analysis for $|11\rangle$ state, we calculate the transformation of the $|2::2\rangle$ state after a beam splitter,

$$\begin{aligned}&\frac{1}{\sqrt{2}}(|20\rangle_{ab}+|02\rangle_{ab})\\&\quad\to\frac{1}{\sqrt{2}}[(t^2-r^2)|20\rangle_{ab}-(t^2-r^2)|02\rangle_{ab}+2\sqrt{2}irt|11\rangle_{ab}].\end{aligned} \tag{B3}$$

For distinguishable particles, the beam splitter transformation is

$$\begin{aligned}&\frac{1}{\sqrt{2}}(|1010\rangle_{a_1b_1a_2b_2}+|0101\rangle_{a_1b_1a_2b_2})\\&\to\frac{1}{\sqrt{2}}[(t^2-r^2)|1010\rangle_{a_1b_1a_2b_2}-(t^2-r^2)|0101\rangle_{a_1b_1a_2b_2}\\&\quad+2irt|0110\rangle_{a_1b_1a_2b_2}+2irt|1001\rangle_{a_1b_1a_2b_2}].\end{aligned} \tag{B4}$$

When a balanced beam splitter is used, coincidence probability becomes 1 for both cases, but note that one has which-way information and the other does not. Then, coincidence probability does not give enough information on distinguishability; thus, another measure of entanglement should be considered such as entanglement entropy, as we discuss in Section 4.

APPENDIX C. DENSITY MATRIX OF 2002 STATE

To compute coincidence probability and entanglement entropy, one has to introduce a density matrix defined as an outer product of output states. Density matrix of output state for a $|2::2\rangle$ input in terms of Fock basis has the form with normalization,

$$\rho_{bef}(\tau_c)=\frac{1}{A+B}\begin{pmatrix}A & C(\tau_c)\\ C^*(\tau_c) & B\end{pmatrix}, \tag{C1}$$

where

$$\begin{aligned}A&=\langle 20|\rho_{bef}(\tau_c)|20\rangle=:\rho_{bef,2020}=\left[\int d\omega|p_{out,1}(\omega)|^2\right]^2,\\B&=\rho_{bef,0202}=\left[\int d\omega|p_{out,2}(\omega)|^2\right]^2,\\C(\tau_c)&=\rho_{bef,2002}=\left[\int d\omega p^*_{out,1}(\omega)p_{out,2}(\omega)e^{i\omega\tau_c}\right]^2.\end{aligned} \tag{C2}$$

Note that coincidence probability ($\langle 11|\rho_{bef}|11\rangle$) is zero before the last beam splitter since the modes are decoupled in our system. After the photon state exhibits interference in the last beam splitter, the density matrix $\rho_{af}(\tau_c)$ becomes

$$\begin{aligned}\rho_{af,2020}&=\rho_{af,0202}=-\rho_{af,2002}=-\rho_{af,0220}\\&=\frac{1}{4(A+B)}[A+B-C(\tau_c)-C^*(\tau_c)],\\\rho_{af,2011}&=\rho^*_{af,1120}=-\rho_{af,0211}=-\rho^*_{af,1102}\\&=\frac{i}{2\sqrt{2}(A+B)}[A-B+C(\tau_c)-C^*(\tau_c)],\\\rho_{af,1111}&=\frac{1}{2(A+B)}[A+B+C(\tau_c)+C^*(\tau_c)],\end{aligned} \tag{C3}$$

where each component labels the basis $\{|20\rangle,|11\rangle,|02\rangle\}$. Note that the last term of the above equations indicates the coincidence probability in Eq. (18). This expression can be obtained equivalently using the unitary operator in the operator basis we defined in Eq. (10). The unitary matrix for two particles in the tensor product form reads

$$U\otimes U:=U_2=\frac{1}{2}\begin{pmatrix}1 & i & i & -1\\ i & 1 & -1 & i\\ i & -1 & 1 & i\\ -1 & i & i & 1\end{pmatrix}. \tag{C4}$$

As we consider indistinguishable particles, it can be contracted on the basis of $\{|20\rangle, |11\rangle, |02\rangle\}$,

$$U_2 = \frac{1}{2}\begin{pmatrix} 1 & \sqrt{2}i & -1 \\ \sqrt{2}i & 0 & \sqrt{2}i \\ -1 & \sqrt{2}i & 1 \end{pmatrix}. \tag{C5}$$

One can check that Eq. (C3) is equivalent to $\rho_{\mathrm{af}}(\tau_c) = U_2\rho_{\mathrm{bef}}(\tau_c)U_2^{\dagger}$. The purity $\mathrm{Tr}[\rho^2]$ thus has the form

$$\mathrm{Tr}[\rho^2(\tau_c)] = \frac{A^2 + B^2 + 2|C(\tau_c)|^2}{(A+B)^2} = 1 + 2\frac{|C(\tau_c)|^2 - AB}{(A+B)^2}. \tag{C6}$$

Note that the purity expressions are identical for ρ_{bef} and ρ_{af} due to the property of unitary transform. Positivity of each term in the numerator guarantees positivity of purity, and it turns out to be equal or less than unity because of Hölder's inequality, $AB \geq |C(\tau_c)|^2$ [53].

Entanglement entropy can be obtained from the above ingredients. Tracing out the lower port degree of freedom (b) yields the expression about the reduced density matrix ρ_a,

$$\begin{aligned} S_a &= -\mathrm{Tr}_a[\rho_a \ln(\rho_a)] \\ &= -\frac{A}{A+B}\ln\frac{A}{A+B} - \frac{B}{A+B}\ln\frac{B}{A+B}. \end{aligned} \tag{C7}$$

Note the controlled delay does not affect the entanglement entropy as off-diagonal components C, C^* representing phase mismatches between fields do not play any role; only the relative intensity of two ports determines this entanglement entropy.

Funding. Institute for Basic Science (IBS-R024-Y1, IBS-R024-D1); Australian Research Council (DP190100277).

Disclosures. The authors declare no conflicts of interest.

REFERENCES

1. F. D. M. Haldane and S. Raghu, "Possible realization of directional optical waveguides in photonic crystals with broken time-reversal symmetry," Phys. Rev. Lett. **100**, 013904 (2008).
2. L. Lu, J. D. Joannopoulos, and M. Soljačić, "Topological photonics," Nat. Photonics **8**, 821–829 (2014).
3. T. Ozawa, H. M. Price, A. Amo, N. Goldman, M. Hafezi, L. Lu, M. C. Rechtsman, D. Schuster, J. Simon, O. Zilberberg, and I. Carusotto, "Topological photonics," Rev. Mod. Phys. **91**, 015006 (2019).
4. Z. Wang, Y. D. Chong, J. D. Joannopoulos, and M. Soljačić, "Reflection-free one-way edge modes in a gyromagnetic photonic crystal," Phys. Rev. Lett. **100**, 013905 (2008).
5. Z. Wang, Y. Chong, J. D. Joannopoulos, and M. Soljačić, "Observation of unidirectional backscattering-immune topological electromagnetic states," Nature **461**, 772–775 (2009).
6. D. Smirnova, D. Leykam, Y. Chong, and Y. Kivshar, "Nonlinear topological photonics," Appl. Phys. Rev. **7**, 021306 (2020).
7. T. Ozawa and H. M. Price, "Topological quantum matter in synthetic dimensions," Nat. Rev. Phys. **1**, 349–357 (2019).
8. G. Harari, M. A. Bandres, Y. Lumer, M. C. Rechtsman, Y. D. Chong, M. Khajavikhan, D. N. Christodoulides, and M. Segev, "Topological insulator laser: theory," Science **359**, eaar4003 (2018).
9. M. A. Bandres, S. Wittek, G. Harari, M. Parto, J. Ren, M. Segev, D. N. Christodoulides, and M. Khajavikhan, "Topological insulator laser: experiments," Science **359**, eaar4005 (2018).
10. Y. Ota, K. Takata, T. Ozawa, A. Amo, Z. Jia, B. Kante, M. Notomi, Y. Arakawa, and S. Iwamoto, "Active topological photonics," Nanophotonics **9**, 547–567 (2020).
11. Z. Gong, Y. Ashida, K. Kawabata, K. Takasan, S. Higashikawa, and M. Ueda, "Topological phases of non-Hermitian systems," Phys. Rev. X **8**, 031079 (2018).
12. S. Mittal, E. A. Goldschmidt, and M. Hafezi, "A topological source of quantum light," Nature **561**, 502–506 (2018).
13. J.-L. Tambasco, G. Corrielli, R. J. Chapman, A. Crespi, O. Zilberberg, R. Osellame, and A. Peruzzo, "Quantum interference of topological states of light," Sci. Adv. **4**, eaat3187 (2018).
14. A. Blanco-Redondo, B. Bell, D. Oren, B. J. Eggleton, and M. Segev, "Topological protection of biphoton states," Science **362**, 568–571 (2018).
15. M. Wang, C. Doyle, B. Bell, M. J. Collins, E. Magi, B. J. Eggleton, M. Segev, and A. Blanco-Redondo, "Topologically protected entangled photonic states," Nanophotonics **8**, 1327–1335 (2019).
16. C. Gneiting and F. Nori, "Disorder-induced dephasing in backscattering-free quantum transport," Phys. Rev. Lett. **119**, 176802 (2017).
17. A. Streltsov, G. Adesso, and M. B. Plenio, "Colloquium: quantum coherence as a resource," Rev. Mod. Phys. **89**, 041003 (2017).
18. E. Joos, H. D. Zeh, C. Kiefer, D. J. Giulini, J. Kupsch, and I.-O. Stamatescu, *Decoherence and the Appearance of a Classical World in Quantum Theory* (Springer, 2013).
19. C. M. Kropf, C. Gneiting, and A. Buchleitner, "Effective dynamics of disordered quantum systems," Phys. Rev. X **6**, 031023 (2016).
20. M. C. Rechtsman, Y. Lumer, Y. Plotnik, A. Perez-Leija, A. Szameit, and M. Segev, "Topological protection of photonic path entanglement," Optica **3**, 925–930 (2016).
21. S. Mittal, V. V. Orre, and M. Hafezi, "Topologically robust transport of entangled photons in a 2D photonic system," Opt. Express **24**, 15631–15641 (2016).
22. C. Gneiting, D. Leykam, and F. Nori, "Disorder-robust entanglement transport," Phys. Rev. Lett. **122**, 066601 (2019).
23. L. Yuan, Q. Lin, A. Zhang, M. Xiao, X. Chen, and S. Fan, "Photonic gauge potential in one cavity with synthetic frequency and orbital angular momentum dimensions," Phys. Rev. Lett. **122**, 083903 (2019).
24. M. Hafezi, E. A. Demler, M. D. Lukin, and J. M. Taylor, "Robust optical delay lines with topological protection," Nat. Phys. **7**, 907–912 (2011).
25. M. Hafezi, S. Mittal, J. Fan, A. Migdall, and J. M. Taylor, "Imaging topological edge states in silicon photonics," Nat. Photonics **7**, 1001–1005 (2013).
26. S. Mittal, J. Fan, S. Faez, A. Migdall, J. M. Taylor, and M. Hafezi, "Topologically robust transport of photons in a synthetic gauge field," Phys. Rev. Lett. **113**, 087403 (2014).
27. S. Mittal, S. Ganeshan, J. Fan, A. Vaezi, and M. Hafezi, "Measurement of topological invariants in a 2D photonic system," Nat. Photonics **10**, 180–183 (2016).
28. L.-H. Wu and X. Hu, "Scheme for achieving a topological photonic crystal by using dielectric material," Phys. Rev. Lett. **114**, 223901 (2015).
29. Y. Plotnik, M. A. Bandres, S. Stützer, Y. Lumer, M. C. Rechtsman, A. Szameit, and M. Segev, "Analogue of Rashba pseudo-spin-orbit coupling in photonic lattices by gauge field engineering," Phys. Rev. B **94**, 020301 (2016).
30. E. Lustig, S. Weimann, Y. Plotnik, Y. Lumer, M. A. Bandres, A. Szameit, and M. Segev, "Photonic topological insulator in synthetic dimensions," Nature **567**, 356–360 (2019).
31. Y. E. Kraus, Y. Lahini, Z. Ringel, M. Verbin, and O. Zilberberg, "Topological states and adiabatic pumping in quasicrystals," Phys. Rev. Lett. **109**, 106402 (2012).
32. C. H. L. Quay, T. L. Hughes, J. A. Sulpizio, L. N. Pfeiffer, K. W. Baldwin, K. W. West, D. Goldhaber-Gordon, and R. de Picciotto, "Observation of a one-dimensional spin orbit gap in a quantum wire," Nat. Phys. **6**, 336–339 (2010).
33. J. Han, C. Gneiting, and D. Leykam, "Helical transport in coupled resonator waveguides," Phys. Rev. B **99**, 224201 (2019).
34. C. Hong, Z. You, and L. Mandel, "Nonclassical photon interference effects," in *Photons and Quantum Fluctuations* (1988), Vol. **5**, p. 51.
35. A. Yariv, Y. Xu, R. K. Lee, and A. Scherer, "Coupled-resonator optical waveguide: a proposal and analysis," Opt. Lett. **24**, 711–713 (1999).

36. D. Leykam, S. Mittal, M. Hafezi, and Y. D. Chong, "Reconfigurable topological phases in next-nearest-neighbor coupled resonator lattices," Phys. Rev. Lett. **121**, 023901 (2018).
37. K. Gottfried and T.-M. Yan, *Quantum Mechanics: Fundamentals* (Springer, 2003).
38. A. Canciamilla, M. Torregiani, C. Ferrari, F. Morichetti, R. M. De La Rue, A. Samarelli, M. Sorel, and A. Melloni, "Silicon coupled-ring resonator structures for slow light applications: potential, impairments and ultimate limits," J. Opt. **12**, 104008 (2010).
39. C. W. Gardiner and M. J. Collett, "Input and output in damped quantum systems: quantum stochastic differential equations and the master equation," Phys. Rev. A **31**, 3761–3774 (1985).
40. F. Schwabl, *Advanced Quantum Mechanics* (Springer, 1997).
41. R. Loudon, *The Quantum Theory of Light* (Oxford University, 2000).
42. A. M. Brańczyk, "Hong-Ou-Mandel interference," arXiv:1711.00080 (2017).
43. J. G. Titchener, M. Gräfe, R. Heilmann, A. S. Solntsev, A. Szameit, and A. A. Sukhorukov, "Scalable on-chip quantum state tomography," npj Quantum Inf. **4**, 19 (2018).
44. M. Zych, "Quantum systems under gravitational time dilation," Ph.D. thesis (University of Vienna, 2015).
45. T. Legero, T. Wilk, A. Kuhn, and G. Rempe, "Time-resolved two-photon quantum interference," Appl. Phys. B **77**, 797–802 (2003).
46. X. Y. Zou, L. J. Wang, and L. Mandel, "Induced coherence and indistinguishability in optical interference," Phys. Rev. Lett. **67**, 318–321 (1991).
47. G. Weihs and A. Zeilinger, "Photon statistics at beam-splitters: an essential tool in quantum information and teleportation," in *Coherence and Statistics of Photons and Atoms* (Wiley, 2001), pp. 262–288.
48. H. Lee, P. Kok, and J. P. Dowling, "A quantum Rosetta stone for interferometry," J. Mod. Opt. **49**, 2325–2338 (2002).
49. S. Paesani, M. Borghi, S. Signorini, A. Maïnos, L. Pavesi, and A. Laing, "Near-ideal spontaneous photon sources in silicon quantum photonics," Nat. Commun. **11**, 2505 (2020).
50. S. Slussarenko, M. M. Weston, H. M. Chrzanowski, L. K. Shalm, V. B. Verma, S. W. Nam, and G. J. Pryde, "Unconditional violation of the shot-noise limit in photonic quantum metrology," Nat. Photonics **11**, 700–703 (2017).
51. M. A. Nielsen and I. Chuang, *Quantum Computation and Quantum Information* (AAPT, 2002).
52. S. Sadana, D. Ghosh, K. Joarder, A. N. Lakshmi, B. C. Sanders, and U. Sinha, "Near-100% two-photon-like coincidence-visibility dip with classical light and the role of complementarity," Phys. Rev. A **100**, 013839 (2019).
53. E. De Faria and W. De Melo, *Mathematical Aspects of Quantum Field Theory* (Cambridge University, 2010), Vol. **127**.